Chapter 2
Terahertz Optics

J Anthony Murphy and Créidhe O'Sullivan

Abstract This chapter covers the basic principles of terahertz (THz) optics, beginning with a review of Gaussian beam propagation and including a section on the design of quasi-optical systems. We review the range of optical components and subsystems typically encountered, and discuss the limitations of practical systems. A section on higher precision modelling is also included that summarises techniques for the analysis of aberration, truncation and cross-polarisation effects.

2.1 Introduction—Optics at THz Frequencies

In this chapter we will look in particular at THz optics, design and modelling. Sandwiched between the optical and microwave regimes, the THz portion of the electromagnetic spectrum with frequencies in the range 300 GHz–3 THz (wavelength 1 mm–100 μm, sometimes up to 10 THz) is a challenging one in which to work and so technologies and analysis techniques are often borrowed from other bands. The lack of readily available THz sources and detectors has led to this relatively unexplored region of the electromagnetic spectrum being termed the "THz gap" [1]. Most of the radiation emitted in the universe since the Big Bang is in this range but at these frequencies the Earth's atmosphere is a strong absorber, mainly due to the presence of water vapour.

Although radiation is typically propagated and analysed as free-space beams, unlike traditional optics, beams may be only a few wavelengths in diameter and diffraction effects can become important [2, 3]. Modelling such beams requires a different approach to geometrical optics, commonly used in the visible where wave-

J. A. Murphy (✉) · C. O'Sullivan
Department of Experimental Physics,
NUI Maynooth, Kildare, Co Kildare, Ireland
e-mail: anthony.murphy@nuim.ie

C. O'Sullivan
e-mail: creidhe.osullivan@nuim.ie

K.-E. Peiponen et al. (eds.), *Terahertz Spectroscopy and Imaging*,
Springer Series in Optical Sciences 171, DOI: 10.1007/978-3-642-29564-5_2,

lengths are assumed to be negligible when compared with component and beam sizes. On the other hand, the physical optics techniques used for radio and microwave systems [4], although very accurate, can be computationally slow and inefficient in the design and analysis process of multi-element systems. A Gaussian beam mode analysis, the basis for most of the discussion on optical design and analysis in this chapter, is a useful compromise between the two. The technique, originally developed for dealing with laser beam propagation, is based on a modal description of electromagnetic field propagation [5] and is appropriate for the description of compact optical systems in which diffraction effects are inevitably important (so called "quasi-optical systems") [3, 6–8].

2.2 Gaussian Beam Propagation in Ideal Optical Systems

2.2.1 Propagation Properties of a Simple Gaussian Beam Mode

In general, Gaussian beam modes are solutions to the paraxial wave equation such that the form of the mode (i.e. intensity distribution) does not change with propagation. They constitute a very convenient basis set of fields with which to simulate the behaviour of propagating beams in quasi-optical systems. The theory of Gaussian beam mode propagation for long-wavelength systems has been elaborated on by a number of authors [1, 3, 6–10] and is the basis for the discussion here.

We begin by assuming quasi-collimated propagation of a monochromatic and spatially coherent beam. Such a paraxial beam travels in a well-defined direction and is by definition of finite transverse extent (and not an infinite plane wave, for example). Thus, for a component E of the complex electric field that satisfies the time-independent wave equation (i.e. the Helmholtz Equation: $\nabla^2 E + k^2 E = 0$ where $k = \omega/c = 2\pi/\lambda$), we search only for paraxial solutions travelling in the z-direction, where the amplitude of the electric field varies gradually over a number of wavelengths in the x- and y-directions and the z-direction variation is still dominated by a term of the form $\exp(-jkz)$. Then re-writing the electric field as $E(x, y, z) \equiv u(x, y, z)\exp(-jkz)$ we can re-express the Helmholtz equation as $\nabla^2 u - 2jk\partial u/\partial z = 0$. For paraxial behaviour $u(x, y, z)$ can only change slowly with z over many wavelengths implying: $|\partial^2 u/\partial z^2| \ll |k\partial u/\partial z|$, thus yielding the so-called paraxial wave equation: $\partial^2 u/\partial x^2 + \partial^2 u/\partial y^2 - 2jk\partial u/\partial z = 0$, which relates how u varies with z in the longitudinal direction to how it varies with x and y in the transverse directions.

It is easy to show that a simple solution for u can be written down in the form

$$u(x, y, z) = \frac{u_0}{(q_0 + z)} \exp\left(-j\frac{k(x^2 + y^2)}{2(q_0 + z)}\right), \tag{2.1}$$

where u_0 and q_0 are constants. Clearly at $z = 0$ we obtain a Gaussian-shaped beam if we choose $q_0 = jkW_0^2/2$ (i.e. q_0 is pure imaginary so that $u(x, y, z) \propto$

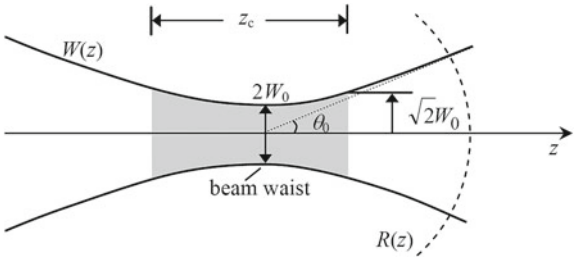

Fig. 2.1 Characteristic parameters of a Gaussian beam

$\exp\left(-(x^2+y^2)/W_0^2\right)$, a Gaussian-shaped intensity pattern with a 1/e in amplitude beam radius of W_0 and a planar phase front. On propagating away from $z = 0$ the exponent in the expression for $u(x, y, z)$ has both real and imaginary terms in $(x^2 + y^2)$, the off-axis transverse distance squared. The imaginary part corresponds to a parabolic phase front on the axis. This has the usual quadratic variation in x and y that one gets in paraxial approximations to a spherical wave front. Re-expressed in the more familiar form

$$E_G(x, y, z) = \sqrt{\frac{2}{\pi W^2(z)}}\exp\left[-\frac{(x^2+y^2)}{W^2(z)} - jk\left(z + \frac{(x^2+y^2)}{2R(z)}\right) + j\phi_0(z)\right], \tag{2.2}$$

where the field has been normalised so that $\int_0^\infty \int_0^\infty |E(x, y)|^2 dxdy = 1$.

Setting $z_c = kW_0^2/2$, the $1/e$ beam width parameter $W(z)$ obeys the relationship $W^2(z) = W_0^2\left(1 + (z/z_c)^2\right)$ while for the phase radius of curvature $R(z) = z + z_c^2/z$. The phase-slippage term $\phi_0(z)$ can be re-expressed as $\phi_0(z) = \tan^{-1}(z/z_c)$, (so called as it represents the phase slippage with respect to a plane wave $E = E_0\exp(-jkz)$ travelling in the z-direction). This may be important in interferometers, for example, in which split beams are recombined after travelling different path lengths so that the phase slippage term is not the same for the two paths.

The beam has a beam waist radius, W_0, at $z = 0$, where by definition it is of minimum extent and also has an infinite radius of curvature (i.e. has a plane wave front). The wave remains quasi-collimated (i.e. $W(z)$ only increases by a factor of less than $\sqrt{2}$) for values of $-z_c < z < z_c$, known as the confocal distance (or Rayleigh range, see Fig. 2.1). This also represents the "depth of focus" of the beam in some sense although the term focus here does not imply an image. The phase slippage varies only gradually with z between the beam waist and the far field (at which point it settles down to $\pi/2$). The paraxial wave equation thus forces the simplest Gaussian beam solution to have certain characteristic parameters: $W(z)$, $R(z)$, $\phi(z)$, which vary with z in a particular way and thus determine its propagation properties.

If we regard E (complex) as representing the electric field, then the power flux $I = \langle \mathbf{E} \times \mathbf{H}^* \rangle = |E|^2/2\mu_0 c$ (i.e. power per unit area). For convenience we drop the $2\mu_0 c$ and normalise the mode so that the so-called "generalised" power given by: $P = \int_S (|E|^2/2\mu_0 c) dS$ is unity, where S is a transverse plane surface.

Because of the scalar nature of the treatment here, E cannot in reality represent the electric field fully. Instead one can think of it as representing the dominant (for example, the co-polar) component. In fact each component of **E** satisfies the wave equation separately and we can use Maxwell's equations to derive all the components of **E** and **H** if we know two of the components (as the case with waveguide modes [11]). Thus, for cases where detailed information about the polarisation properties of a beam is of interest a vector approach is necessary. It is also possible to carry out a Gaussian beam mode analysis for both transverse components E_x and E_y independently and thus include polarisation at the level of approximation of paraxial optics, although in this case Maxwell's equations are not strictly satisfied [7, 12].

It is worth noting that the same approximations are valid for Gaussian beam mode propagation as for the Fresnel diffraction approximation [7, 9]. In fact we can model both the Fresnel and Fraunhofer regions conveniently with a Gaussian beam mode analysis [13]. Often a simple Gaussian mode is a good approximation both to the radiated beam produced by a typical THz source and to the reception pattern of a typical detector feed, as discussed later. This allows one to readily design optical systems to guide and re-collimate the propagating beam as required for a compact and efficient design [6].

2.2.2 Focussing Gaussian Beams: Simple Optical Systems

A Gaussian beam can be re-collimated using a re-focussing element such as a simple thin lens or curved mirror acting as a phase transformer operating on the spherical incident wavefront of the beam [3, 10]. The correct approach is to regard the effect of an ideal thin lens placed in the path of a Gaussian beam as transforming the radius of curvature R_{in} of the incident wavefront to R_{out} for the transmitted wavefront according to the relationship $1/R_{\text{out}} = 1/R_{\text{in}} - 1/f$, where f is the focal length of the focussing component. In this formalism, we regard R_{out} as negative if the centre of curvature lies at a more positive value of z than the plane of interest [6]. Clearly, once the power of the thin lens is high enough, we can re-collimate or re-focus a beam. Thus, by appropriate combination of phase curvature transformations we can maintain a quasi-collimated beam over a long distance using a series of re-focussing thin lenses to form a so-called beam guide.

For Gaussian beams, however, the phase radius of curvature R is generally not equal to the distance back to the beam waist or "focus", which complicates optical system design when dealing with Gaussian beams. Clearly, therefore, the usual formulas for imaging in geometrical optics cannot be used in long-wavelength systems to predict the position of the beam waists. At short wavelengths a focussing thin lens of sufficient power will form an image of a point source (a distance u from the thin lens) at a distance $v = uf/(u - f)$ from the thin lens, whereas at long wavelengths $R_{\text{in}} \neq d_{\text{in}}$ and $R_{\text{out}} \neq d_{\text{out}}$, where d_{in} and d_{out} are the respective distances back to the respective beam waists. In fact it is important to make a distinction between forming a beam waist (beam at its narrowest extent) and re-imaging the amplitude pattern of a

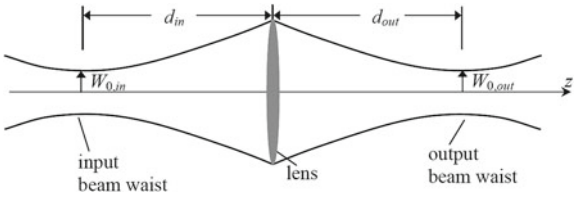

Fig. 2.2 The focussing of a Gaussian beam

single beam with a complex structure, or indeed even re-imaging an array of beams. A complex field pattern at some plane, even if at a beam waist, will not generally be re-imaged at another beam waist, except for very specialised optical systems such as Gaussian beam telescopes to be discussed below in this section. In general for single-beam systems in which a simple Gaussian beam propagates, imaging issues do not have to be considered.

Given that the width of the transmitted beam at an ideal thin lens (i.e. a planar phase transformation) must match that of the incident beam allows us to derive some useful relationships for the position and width of the beam waist on the output side $W_{0,\mathrm{out}}$ (see Fig. 2.2), where in terms of the incident beam width parameter $W_{0,\mathrm{in}}$ and the focal length of the thin lens (as given in [3, 6] for example)

$$W_{0,\mathrm{out}}^2 = \frac{W_{0,\mathrm{in}}^2}{\left(1-\frac{d_{\mathrm{in}}}{f}\right)^2 + \left(\frac{kW_{0,\mathrm{in}}^2}{2f}\right)^2} \quad \text{and} \quad d_{\mathrm{out}} = f + \frac{d_{\mathrm{in}} - f}{\left(1-\frac{d_{\mathrm{in}}}{f}\right)^2 + \left(\frac{kW_{0,\mathrm{in}}^2}{2f}\right)^2}. \tag{2.3}$$

On considering these, an interesting solution arises if $d_{\mathrm{in}} = f$, as then also $d_{\mathrm{out}} = f$ (independent of input beam parameters or wavelength!) and both beam waists are on the focal planes of the focussing thin lens and satisfy $W_{0,\mathrm{out}} W_{0,\mathrm{in}} = (2f/k) = (\lambda f)/\pi$. This behaviour is in marked contrast to geometrical optics and illustrates typical pitfalls in long-wave optics if a geometricl optics design is assumed adequate.

A very convenient optical system is obtained if we arrange a pair of thin lenses separated by the sum of their focal lengths $f_1 + f_2$ with the input beam waist at the focal plane of the first thin lens (of focal length f_1). In this case the output beam waist at thin lens 2 (of focal length f_2), the output focal plane of the system, becomes *independent of frequency*. The system has the optical configutation of a perfect classical optical telescope where $d_{\mathrm{out}} = f_2$ and $W_{0,\mathrm{out}} = (f_2/f_1)W_{0,\mathrm{in}}$! In fact this arrangement is known as a Gaussian beam telescope.These have very important applications in long-wave optical systems particularly where wide-bandwidth behaviour is required. In a multi-element thin lens system we can build up a beam guide by cascading Gaussian beam telescopes thus producing a broadband arrangement that is independent of frequency and has constant magnification if all focal lengths are equal.

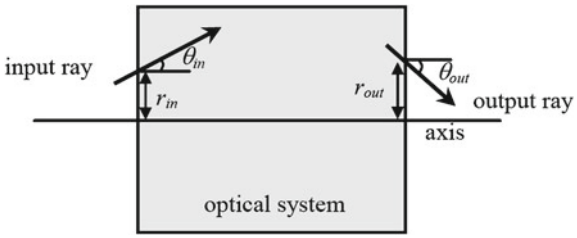

Fig. 2.3 Input and output ray trajectories defined by $(r_{\text{in}}, \theta_{\text{in}})$ and $(r_{\text{out}}, \theta_{\text{out}})$

2.2.3 ABCD Matrices and Propagation in General Optical Systems

For multi-element optical systems we can use the convenient *ABCD* ray transfer matrix formalism commonly used in geometrical optics [3, 5, 10]. In this case the *ABCD* transfer matrix **M** operates on a vector made up of r, the distance from the optical axis to a point on the ray trajectory and the angle θ it makes with the axis (see Fig. 2.3), transforming $(r_{\text{in}}, \theta_{\text{in}})$ at the input reference plane into $(r_{\text{out}}, \theta_{\text{out}})$ at the output reference plane according to the matrix equation

$$\begin{bmatrix} r_{\text{out}} \\ \theta_{\text{out}} \end{bmatrix} = \mathbf{M} \cdot \begin{bmatrix} r_{\text{in}} \\ \theta_{\text{in}} \end{bmatrix} = \begin{bmatrix} A & B \\ C & D \end{bmatrix} \cdot \begin{bmatrix} r_{\text{in}} \\ \theta_{\text{in}} \end{bmatrix} = \begin{bmatrix} Ar_{\text{in}} + B\theta_{\text{in}} \\ Cr_{\text{in}} + D\theta_{\text{in}} \end{bmatrix}. \tag{2.4}$$

For a multi-element system made up of a series of thin lenses and other optical components, the full *ABCD* matrix is given by a simple matrix product of the corresponding *ABCD* matrix for the individual components but taking care to include any distance propagated in free space or in a medium between components.

The connection with a Gaussian beam is made through the effect of an optical system on the phase curvature of the beam [5]. At short wavelengths a spherical wave emanating from a point source on the optical axis of the system can be modelled as a fan of rays impinging on the input plane where for each ray $r_{\text{in}}/\theta_{\text{in}} = R_{\text{in}}$ is a constant which corresponds to the radius of curvature of the phase front and is equal to the distance back to the point source. Thus, the relationship between the input plane and output plane phase curvatures can readily be derived, $R_{\text{out}} = r_{\text{out}}/\theta_{\text{out}} = (AR_{\text{in}} + B)/(CR_{\text{in}} + D)$. The *ABCD* matrix formalism for tracing rays thus allows one calculate how the radius of curvature for this beam varies with propagation through the optical system.

Analogously a Gaussian beam can be treated as a complex point source with complex radius of curvature $q(z) = q_0 + z$ on re-expressing the equation for a simple Gaussian as $u(x, y, z) \propto \exp\left(-jk(x^2 + y^2)/2q(z)\right)$, consistent with Eq. 2.1. The same relationship can be applied in this case to the *complex* phase radius of curvature term q_{in} on propagation of a Gaussian beam from the input to the output plane of some component, $q_{\text{out}} = (Aq_{\text{in}} + B)/(Cq_{\text{in}} + D)$, where q_{out} is the complex radius of curvature at the output plane. We can then recover $(W_{\text{out}}, R_{\text{out}}, \phi_{\text{out}})$ at the output plane for a given $(W_{\text{in}}, R_{\text{in}}, \phi_{\text{in}})$ at the input plane, where $1/q_{\text{in}} = 1/R_{\text{in}} - j\lambda/\pi W_{\text{in}}^2$. The recovered beam parameters at the ouput plane are

Table 2.1 Examples of *ABCD* matrices

	ABCD Matrix **M**
Propagation a distance L in free space (or a medium of constant refractive index)	$\begin{bmatrix} 1 & L \\ 0 & 1 \end{bmatrix}$
Transformation at a thin lens of focal length f	$\begin{bmatrix} 1 & 0 \\ -1/f & 1 \end{bmatrix}$
Transformation for a Gaussian beam telescope with thin lenses of focal lengths f_1 and f_2	$\begin{bmatrix} -f_2/f_1 & 0 \\ 0 & -f_1/f_2 \end{bmatrix}$
Refraction at a curved interface of radius of curvature R (where n_1 is the initial refractive index, n_2 is the final refractive index, $R < 0$ for convex (centre of curvature after interface))	$\begin{bmatrix} 1 & 0 \\ -(n_1 - n_2)/Rn_2 & n_1/n_2 \end{bmatrix}$

$$R_{\text{out}} = \left(\text{Re}\left[\frac{C + D/q_{\text{in}}}{A + B/q_{\text{in}}}\right]\right)^{-1} \quad W_{\text{out}} = \sqrt{\frac{-\lambda}{\pi}\left(\text{Im}\left[\frac{C + D/q_{\text{in}}}{A + B/q_{\text{in}}}\right]\right)^{-1}}$$
$$\phi_{0,\text{out}} = \phi_{0,\text{in}} - \text{Arg}\left[A + B(1/q_{\text{in}})\right]. \tag{2.5}$$

The *ABCD* matrices for a number of important examples are given in Table 2.1. If a beam propagates through several optical elements (and we include diffraction effects over the path lengths between the componenets) a single *ABCD* matrix may be computed for the system, which is the matrix product of all the individual matrices. The first optical element must be on the right-hand side of that product.

$$\mathbf{M}_{\text{total}} = \mathbf{M}_N \cdot \mathbf{M}_{N-1} \cdot \ldots \cdot \mathbf{M}_2 \cdot \mathbf{M}_1 = \begin{bmatrix} A & B \\ C & D \end{bmatrix}_{\text{total}}. \tag{2.6}$$

This turns out to be a very powerful technique in designing quasi-optical systems. In the next section we consider the practical issues that arise with re-imaging beams using both focussing mirrors and thick lenses, as well as other optical devices which can be used for developing sophisticated quasi-optical "circuits".

2.3 Optical Components and Subsystems

2.3.1 Coupling Beams and Focussing Elements

In general when coupling a source to a detector we have to ensure that the source beam is well matched to the reception beam of the detector feed antenna. Any mismatches will give rise to power losses and partial reflections with a reduction in performance. To a reasonable level of accuracy we can design a system with acceptable optical

performance if we can assume that a simple Gaussian beam approximation is valid and that the focussing elements to re-collimate and re-focus the beam are ideal.

In practical applications both re-focussing mirrors as well as lenses tend to be used as phase curvature transformers. Lenses can be easily manufactured from various plastic materials with convenient indices of refraction for the purpose, along with other dielectric and semiconductor materials such a quartz, fused silica, saphire and silicon [1]. However, some potentially useful materials have non-ideal properties such as non-negligible loss tangents. Also, unless anti-reflection coated, the air–dielectric interface can give rise to partial reflections, especially for materials with high refractive indices such as silicon. Furthermore, any nonuniformities in such materials will introduce extra aberrations and possible cross-polarisation effects which are difficult to model. Useful discussions and reviews are to be found in [3]. Also the recent development of artifical materials including metamaterials at THz frequencies holds out the promise of high resolution imaging [1].

Off-axis focussing mirrors are often preferred for re-collimating the beams because the optical behaviour of the lenses are so affected by the material properties. Although such mirrors do introduce some distortion and cross-polarisation effects, such effects can be precisely modelled and the resulting non-ideal effects predicted [14, 15]. Off-axis mirrors are also easy to manufacture from inexpensive materials, and because the mirror deflects a beam, they lend themselves to compact folded optical systems. For high-sensitivity applications it is possible to cryogenically cool mirrors.

As well as guiding waves using beam guides based on focussing optical components, waveguides and optical fibres (including bare metal wires as effective waveguides) may also be employed depending on the application [16].

Other imaging modalities based on holographic techniques are reported for example in [17, 18]. Such an approach can be used to recover THz images of an actively illuminated object, including phase information. The technique relies on the interefference of the object beam with a reference beam, both derived from the same coherent source.

2.3.2 Off-Axis Focussing Mirrors

Off-axis ellipsoidal and parabolic mirrors are often used for re-focussing beams. An ellipsoid of revolution provides the ideal phase transformer for matching an input and output spherical wavefront. Projection effects may give rise to some slight asymmetric distortion of the amplitude which can usually be neglected [14, 15]. The centres of curvature of these spherical phase surfaces should coincide with the corresponding foci of the ellipsoid (see Fig. 2.4) [3]. If we wish to re-focus and deflect the beam, and the phase radii of curvature at the point where the deflected beam axis interesects the mirror surface are given by $R_{\text{in}} = R_1$ and $R_{\text{out}} = -R_2$, then the semi-major axis of the appropriate ellipsoid is given by $a = (R_1 + R_2)/2$, while the semi-minor axis is $b = \sqrt{R_1 R_2}\cos\theta_i$, where θ_i is the angle of incidence

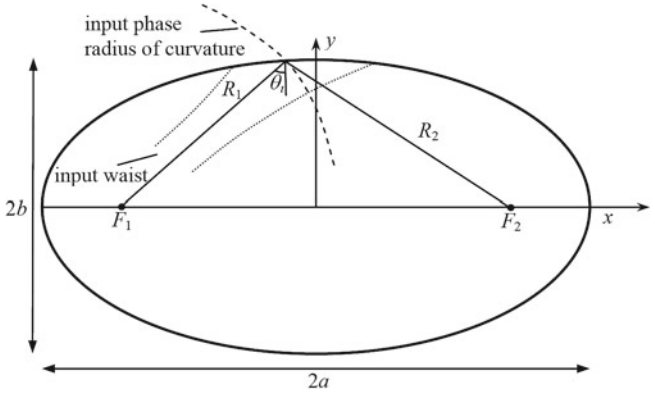

Fig. 2.4 Ellipsoid with foci at F_1 and F_2

(half the deflection angle) and the usual equation for an ellipse applies: $x^2/a^2 + y^2/b^2 = 1$, with the actual mirror surface part of a surface of revolution around the x- axis as shown in the figure. The focal length of an ellipsoidal mirror is given by $1/f = 1/R_1 + 1/R_2$ so that the mirror effectively behaves as a thin lens. Note of course that the beam waists do not coincide with the geometrical foci of the ellipse F_1 or F_2 (see Fig. 2.4). Instead, the distance back to the input beam waist is given by: $d_{\text{in}} = R_{\text{in}}/[1 + (\lambda R_{\text{in}}/\pi W_m^2)^2] < R_1$, where W_m is the beam width parameter at the mirror.

If the input or output beam waist is at the mirror itself then the appropriate mirror reduces to an off-axis parabolic mirror (i.e. the limit for an ellipsoid when R_1 or R_2 is very large). The mirror produces a perfect phase transformation between a spherical and a plane wave front, although projection effects again give rise to some asymmetric distortion on reflection [15]. A parabolic (or more strictly paraboloidal) mirror is the correct conic reflecting surface for a large beam waist at the mirror (plane wavefront) imaged to narrower beam waist near the geometrical focus of parabola (typical in astronomical telescopes etc.). Given R_1 and the angle of incidence θ_i we can determine the correct paraboloidal surface (paraboloid of revolution around x-axis where $y^2 = 4px$, see Fig. 2.5) with $p = R_1 \cos^2 \theta_i$. Parabolic mirrors are often used as good substitutes for ellipsoidal mirrors if $R_2 \gg R_1$, or vice versa (e.g. if the mirror is in far field of a source or detector, for example).

When dealing with multi-beam systems, off-axis mirrors do introduce significant aberrations and distortion effects across the field of view (region over which beams are spread), especially away from the optical axis of the system. In that case very careful optical design is necessary to reduce the phase aberrations across the field of beams while at the same time properly accounting for the dominant diffraction effects. This is solved using an approach which couples design-technique principles from both optical engineering (and normally applied at short wavelengths) along with long-wave optics leading to compensated systems, e.g. the Planck satellite focal plane [19]. Also, for example, in specialised systems cross-polar effects can

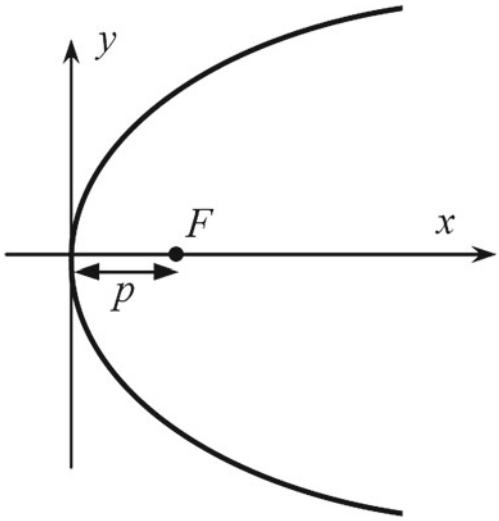

Fig. 2.5 Paraboloid with focus at F

be minimised using so-called Dragone-Mitzsugushi configurations [20]. However, these effects are not generally a significant issue for single beam systems where a small amount of beam squint can be tolerated [15]. There is further discussion on these points in the section on the design of optical systems, particularly for broadband THz spectroscopy systems, where the use of parabolic mirrors is popular.

2.3.3 Thick Lenses

There will be some diffraction effects associated with the transmission of a beam through a thick lens. We can derive the *ABCD* transformation matrix $\mathbf{M}_{\text{thick lens}}$ for a thick lens with spherical surfaces in a general form. If R_1 and R_2 are the radii of curvatures of the surfaces on the input and output sides, respectively, then this can be written (where d is the lens thickness, n_2 is the refractive index of the lens material and n_1 and n_3 are the refractive indices of the media on the input and output sides, respectively) as:

$$\mathbf{M}_{\text{thick-lens}} = \begin{bmatrix} \frac{n_2R_1-(n_1-n_2)d}{n_2R_1} & \frac{n_1}{n_2}d \\ \frac{n_3-n_2}{n_3R_2} - \frac{n_1-n_2}{n_3R_1} + \frac{(n_3-n_2)(n_2-n_1)n_1d}{n_2n_3R_1R_2} & \frac{n_1(n_2R_2-(n_2-n_3)d)}{n_2n_3R_2} \end{bmatrix}. \quad (2.7)$$

For the case where $n_1 = n_3 = 1$ and $n_2 = n$, the refractive index of the lens material, this yields:

$$\mathbf{M}_{\text{thick-lens}} = \begin{bmatrix} 1 + \frac{(n-1)d}{nR_1} & \frac{d}{n} \\ (n-1)\left(\frac{1}{R_1} - \frac{1}{R_2} - \frac{(n-1)}{n}\frac{d}{R_1 R_2}\right) & 1 - \frac{(n-1)d}{nR_2} \end{bmatrix}. \quad (2.8)$$

Short focal length lenses may require the surface to be shaped to deal with non-paraxial rays in order to reduce aberrations (this is discussed in [3], for example). This would be appropriate when a lens is used at the aperture of a horn antenna. Goldsmith [3] also discusses other refracting focussing elements such as zoned (Fresnel) lenses. Antireflection coatings have been developed particularly for lenses made of high refractive index matrials, e.g. [1, 21, 22].

2.3.4 *Beam Splitters, Polarising Grids, Roof Mirrors, Interferometers and Filters*

Useful components have also been developed which function as optical devices in so-called quasi-optical circuits, mimicking waveguide devices and circuitry. Both frequency-selective devices (e.g. filter plates) and frequency-independent devices (e.g. roof-mirrors) are widely utilised in both frequency-dependent and frequency-independent applications. There is an extensive review of the operation and application of such components in [1, 3], for example. Clearly, as well as their basic function, various aspects of Gaussian beam propagation through such devices need to be considered, such as beam spreading, truncation levels and phase slippage. For example, as a rule of thumb the component should not truncate the beam at a radius of less than 2 beam width parameters, W, otherwise undesired diffraction of the beam as well as loss in transmitted power will occur.

One example of a very useful but simple optical device is the roof mirror, which rotates the direction of polarisation of an incident wave by an angle of 2α, if the angle between the incident polarisation and the axis of the roof mirror is α (see Fig. 2.6). The roof mirror produces the rotation as the field component parallel to the flat surfaces is not affected while the component normal to surface has its direction reversed in the double reflection. When combined with a polarising grid, roof mirrors can be configured as path-length modulators for a single beam [3] or as the polarisation rotation mirrors in a Michelson polarising interferometer (see Fig. 2.6) [23]. In both these applications a polarising grid is present which reflects polarisation parallel to the polarising grid wires and transmits, without significant loss, polarisation perpendicular to the grid wires. Path-length modulators are useful for introducing propagation delays, while polarising Michelson interferometers can be utilised as low-loss beam combiners for two beams closely spaced in frequency (local oscillator injection in heterodyne systems) or as single-sideband filters, e.g. [24] as well as in Fourier transform spectroscopy. Alternatively, a wire-grid attenuator or power divider that is free of reflections back into the incident beam can be designed by using wire grids as beam splitters.

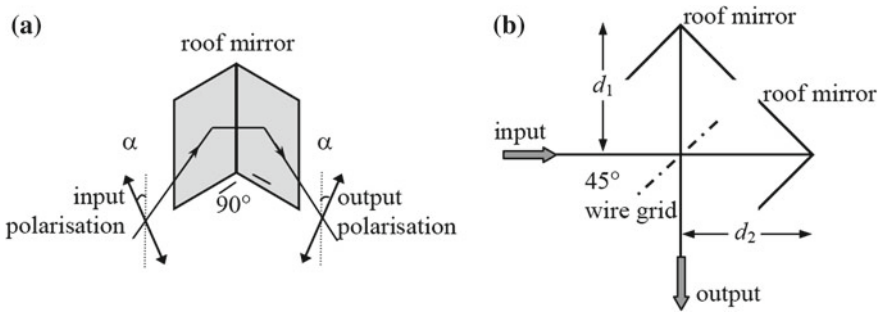

Fig. 2.6 **a** Roof mirror rotating the input polarisation direction and **b** polarisation-rotating interferometer (90° polarisation rotation when $d_1 - d_2 = \lambda/2$)

Polarisation transducers are useful quasi-optical devices that produce an arbitrary differential phase shift between two orthogonal electric-field polarisation directions. For example, a half-wave plate provides a differential phase shift of π between two orthogonal electric field polarisation directions while a quarter-wave plate transforms linear to circular polarisation. Wave plates have artificially generated (through mechanical milling) fast and slow axes (the names refer to the speed of a wave along the axis) [25]. A quasi-optical polariser based on self-complementary subwavelength hole arrays are reported in [26].

It is also possible to make anisotropic materials from one that is naturally isotropic by altering its geometry, thus simulating a birefringent dielectric, for example [27]. Dielectric strips of alternating permitivities can be combined to form composite dielectrics with the required dielectric constant, provided the wavelength is much longer than the strip thickness. Such strips can also be used as filters, mirrors, etc. [28].

Extremely useful high- and low-pass filters can also be made with inductive and capacitative grids, respectively, [29] while resonant grids can be used for band-pass filtering and a perforated plate filter as a high-pass filter with a sharp cutoff, even with profile shaping for lensing [25]. A transmission line matrix method can be used as a convenient way of calculating the frequency response of systems composed of cascaded elements [27].

2.3.5 Diffractive Elements and Phase Gratings

Diffractive optic elements are optical components that redirect segments of a wavefront through the use of interference and/or phase control [30]. They can be used to transform the intensity distribution of a coherent beam of light at one plane into another intensity pattern at a second plane (the far field, for example) by imposing a phase distribution on the field. Examples include the Fresnel phase plate, Dammann

Gratings and Fourier Gratings [31–33] that can be used to generate multiple images of a single input beam. Such devices are useful for quasi-optically multiplexing a local oscillator source with an array of detectors in a heterodyne system. There are a number of dielectric materials whose mechanical and optical properties in the far infrared make them ideal candidates for use in transmission phase gratings [1, 3].

In designing phase gratings, no analytical solution exists for finding the phase profile required to transform a given arbitrary input field to a given arbitrary output field, and in fact an exact transform may not even be possible [34]. Optimisation techniques, such as simulated annealing or genetic algorithms, and phase-retrieval techniques such as the Gerchberg-Saxton algorithm have all been applied to find optimal phase solutions [35, 36].

Another useful example of beam-shaping is in the production of "diffraction-free beams", in which the amplitude does not change in form or scale while propagating [37]. These beams have an amplitude cross-section of a Bessel function and, ideally, are infinite in extent. Pseudo-Bessel beams (having finite extent and power) have been generated using dielectric conical-shaped lenses called axicons [38, 39].

2.4 Beam Coupling Issues

2.4.1 Coupling to Radiating Elements

Many different kinds of radiating elements are used as feed systems for launching and detecting THz waves. These systems ideally produce quasi-Gaussian beams so that the sidelobe content is not very significant and a simple Gaussian beam can be used as a good approximation in designing optical systems and beam guides. For higher levels of accuracy a multi-moded description of the beam can be applied as discussed below (Sect. 2.5.1).

One of the most predictable feed types, in terms of producing a well-controlled and understood beam, is the horn antenna.The field at a horn aperture can be predicted from wave-guide theory, and this is an ideal plane at which to determine the decomposition into higher order modes for a multi-mode analysis. To a good approximation the field at the aperture has a well-defined phase radius of curvature R with the centre of curvature located at the apex of the horn flare. This is true for both the typical conical and pyramidal shapes encountered (i.e. $R = L_{\text{axial}}$, the axial slant length of the horn). Note that in terms of fitting a Gaussian beam to the field, the spherical phase variation off-axis can be expressed using the usual quadratic approximation for paraxial beams, and we choose a value for beam width parameter, W, that optimises coupling to the fundamental, $E(x, y) \approx A_0 E_G(x, y)$, where A_0 is the fundamental mode coefficient and $E_G(x, y)$ is a simple Gaussian (fundamental mode).

For a corrugated horn antenna the beam width at the aperture (radius a) can be set to $W_{\text{ap}} = 0.6435a$, and the phase curvature is given by the horn axial length as

Table 2.2 Gaussian approximation to horn beams

Horn type	Beam width W
Corrugated conical	$0.643a$ (radius) [40]
Smooth walled conical	$0.765a$ (radius) [12]
Rectangular	$0.35a \times 0.51b$ (width $\times$ height) [42]
Diagonal	$0.42a$ (sidelength) [43]

above [40, 41]. This approximate Gaussian fit can be used to represent the actual corrugated horn antenna beam in designing any optical beam guides required. It is worth noting that although the Gaussian is a good fit (with 98 % fractional power coupling) to the beam from a corrugated horn, it cannot represent the side-lobe structure (typically below the -20 dB level). In fact it only poorly predicts the intensity on axis, and only if one calculates the integrated power (inside radius r) is much better agreement obtained between the Gaussian and horn fields. Of course this is what is essentially optimised in finding the "best-fit" Gaussian. In Table 2.2 we list the best-fit Gaussian parameters for typical horn antennas.

The fractional coupling of the lowest order one-dimensional Gaussian mode to a truncated uniform field (of width a) has its maximum value when $W = 0.51a$ and to a simple cosine tapered field when $W = 0.35a$. The fractional coupling of a square TE_{10} waveguide field to the lowest order two-dimensional fundamental Gaussian mode $E_G(x, y)$, with the beam waists in the x and y coordinates equal, has its maximum value when $W = 0.43a$, where a is the sidelength of the square waveguide (the same as for a diagonal horn). In the latter case, 84 % of the power is contained in the fundamental mode, which compares with 98 % for the HE_{11} mode of a corrugated horn antenna.

Clearly one needs to include higher order Gaussian beam modes for a more accurate description of real fields (non-Gaussian effects) in order to simulate how the beam pattern of a horn antenna evolves and develops sidelobe structure for example. These so-called sidelobes are equivalent to subsidiary maxima in classical wave optics, of course, as normally simulated using Fresnel and Fraunhofer diffraction integrals.

Horn antennas become difficult to manufacture at frequencies around 1 THz and above, and other structures including planar lens antenna schemes are often employed [3]. Generally the beams produced by these other structures are not as well behaved, nor indeed as well understood, as the horn antenna feeds and the power coupling to a fundamental Gaussian (the Gaussicity of the beam) will be somewhat lower with higher sidelobe levels. These issues are discussed further in Sect. 2.6.3.

2.4.2 Mismatched Gaussian Beams and Defocussing Effects

In designing quasi-optical systems and analysing potential losses in non-ideal systems, the coupling of beams together becomes an issue (such as how a source beam is matched to a detector, for example). Generally two situations arise: (i) the

coupling of an incident beam from a source to a beam that characterises a component such as a detector or the recombination of a pair of beams in an interferometer such as a Michelson for example, or (ii) the imperfect coupling that occurs because of mechanical misalignment, defocusing or other tolerancing effects in a quasi-optical beam guide.

A beam coupling efficiency analysis requires the calculation of the fraction of power coupled from an incident beam to the beam of the component of interest, as a function of some mismatch between the parameters (W_a, R_a) and (W_b, R_b) of the two beams a and b, respectively. The power coupling coefficient between two fields E_a and E_b over a transverse plane S is defined by the overlap integral $C_{\text{ab}} = \left|\int\int_S E_a^*(x, y; W_a, R_a).E_b(x, y; W_b, R_b)\mathrm{d}x\mathrm{d}y\right|^2$. Since a scalar field has been assumed, one must be careful with polarisation effects and normalisation (as the true field coupling is a vector equation). Here therefore it is assumed that both fields are polarised in the same sense (since we are using a scalar approximation). A number of interesting common cases arise for different kinds of mismatched beams. We will assume that for these cases Gaussian beam approximations are adequate descriptions of the beams, particularly as it is often the order of magnitude of the fractional power coupling loss due to mismatch that is required.

We first consider a defocussed system which occurs when the two beams are axially aligned (optical axes aligned) but the beam waists do not coincide as they should for maximum power coupling (for example the detector feed phase centre is not quite on the focal plane in a telescope system). Thus, there will be a mismatch in the beam width W and phase curvature R at some arbitrary plane. It may also be that the beams have mismatched beam waist sizes (such as a detector feed antenna with the wrong parameters to match the incident source field). For the general case, therefore, neither beam waists coincide nor are the beam waist radii $W_{0,a}$ and $W_{0,b}$ equal. The on-axis phase slippages will be different in general as well, $\phi_{0,a} \neq \phi_{0,b}$, which could be an issue for an interferometer or delay line, for example. For such a mismatched and defocussed system the fractional power coupling can be shown to be expressible in terms of the beam waist parameters and the distance between the beam waist positions as

$$C_{\text{ab}}^{\text{axial}} = \frac{4}{\left(\frac{W_{0,b}}{W_{0,a}} + \frac{W_{0,a}}{W_{0,b}}\right)^2 + \left(\frac{\lambda\Delta z}{\pi W_{0,a} W_{0,b}}\right)^2}, \tag{2.9}$$

where Δz is the shift of the beam waist [3]. Even if the beams are otherwise well matched in terms of their optical parameters, mechanical mismatches may still occur (due to realistic tolerancing errors, for example) which cause the optical axes of the two beams to be misaligned [44]. We can analyse these tolerencing errors in terms of lateral shifts and tilts. Figure 2.7 illustrates defocusing as well as tilt and offset mismatched beams.

In the case of tilts, a mismatch gives rise to a phase slope in one of the fields relative to the other across the plane where their optical axes intersect. For Gaussian beams which have the same beam parameters (no other mismatches other than tilt)

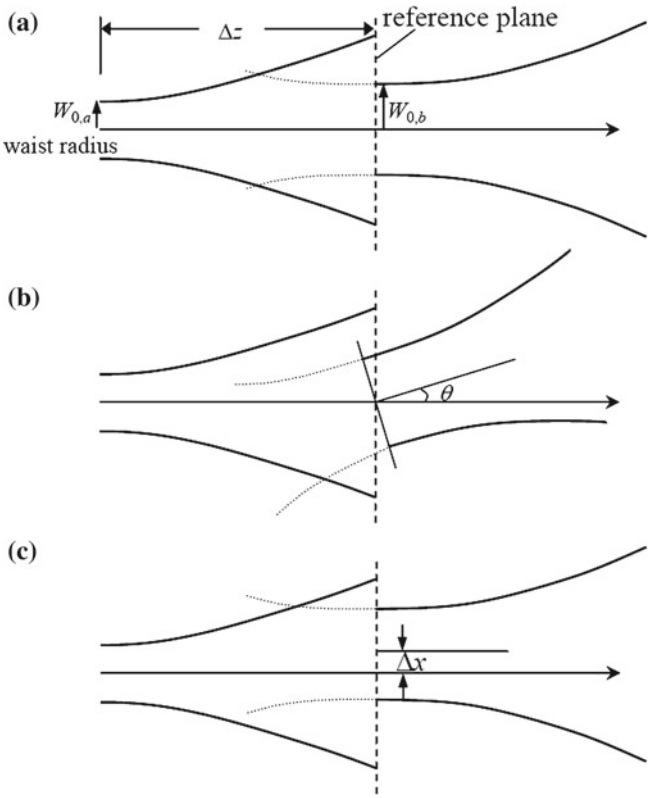

Fig. 2.7 Gaussian beam misalignment: **a** defocus, **b** defocus and tilt, and **c** defocus and off-offset

it can be shown [3] that the fractional power coupling between the beams is given by

$$C_{\text{ab}}^{\text{tilt}} = \exp\left[-\left(\frac{\theta}{\theta_W}\right)^2\right], \tag{2.10}$$

where $\theta_W = \frac{\lambda}{\pi W}$ and where the tilt occurs at the beam waist. For lateral offsets if we assume a beam displacement of Δx in the x direction, (but otherwise beam widths and waist locations are the same), the fractional power coupling including the loss due to offset can be shown to be given by

$$C_{\text{ab}}^{\text{offset}} = \exp\left[-\left(\frac{\Delta x}{W_0}\right)^2\right], \tag{2.11}$$

a similar dependency to that for tilt misalignments. In general more than one type of mismatch may be present particularly when tolerencing errors are large and thus may affect system performance (see Fig. 2.7).

Often for system design or a basic analysis of tolerencing, a simple Gaussian beam mode approach is an excellent compromise in terms of speed of computation particularly for optimisation. When a more precise analysis of loss in a system is required however a full modal description of a beam also including the higher order modes in the analysis may be necessary, as will be discussed in the next section.

2.5 Detailed Modelling

2.5.1 Higher Order Gaussian Beam Modes

A Gaussian beam is the simplest solution to the paraxial wave equation and suffices in many cases to describe beam propagation in an optical system. There are situations, however, when we need to model more complex field distributions and in these cases we can use higher order beam mode solutions (see e.g. [3]). These higher order Gaussian modes are characterised by the same beam radius $W(z)$ and phase radius of curvature $R(z)$ as the fundamental mode, only the phase slippage, (with respect to a plane wave) differs. The most appropriate mode-set to use depends on the symmetry of the system being modelled. In cylindrical coordinates (r, φ, z) we can use Gaussian–Laguerre modes

$$\begin{aligned} E_{\mathrm{pm}}(r,\varphi,z) = &\left[\frac{2p!}{\pi(p+m)!}\right]^{0.5} \frac{1}{W(z)} \left[\frac{\sqrt{2}r}{W(z)}\right]^{m} L_p^m\left(\frac{2r^2}{W^2(z)}\right) \\ &\times \exp\left[\frac{-r^2}{W^2(z)} - jkz - \frac{j\pi r^2}{\lambda R(z)} + j(2p+m+1)\phi_0(z)\right] \\ &\times \exp(jm\varphi), \end{aligned} \tag{2.12}$$

where $L_p^m(s)$ are generalised Laguerre polynomials, and in Cartesian coordinates (x, y, z) Gaussian–Hermite modes

$$\begin{aligned} E_{\mathrm{mn}}(x,y,z) = &\left(\frac{1}{\pi\, W^2(z)\, 2^{m+n-1}\, m!\, n!}\right)^{0.5} H_m\left(\frac{\sqrt{2}x}{W(z)}\right) H_n\left(\frac{\sqrt{2}y}{W(z)}\right) \\ &\times \exp\left[-\frac{x^2+y^2}{W^2(z)} - jkz - \frac{j\pi(x^2+y^2)}{\lambda R(z)} + j(n+m+1)\phi_0(z)\right], \end{aligned} \tag{2.13}$$

where $H_m(t)$ are Hermite polynomials and the modes are normalised so that the generalised power is unity (orthonormal mode sets). ϕ_0 is the usual phase slippage of

the fundamental mode. These higher order solutions consist of polynomials superimposed on the fundamental Gaussian mode and constitute complete orthonomal sets of modes that are each solutions to the paraxial wave equation. Any paraxial beam $E(x, y, z)$ can therefore be expressed as a superposition of Gaussian modes (for example in the case of Cartesian coordinates),

$$E(x, y, z) = \sum_i A_i \; E_i(x, y, z), \tag{2.14}$$

where A_i are the mode coefficients and i represents the pair of indices (m, n) for the mode. If the field is known over the surface S then the mode coefficients are determined by calculating the overlap integrals

$$A_i = \int\int_S E_i(x, y, z)^* E(x, y, z) ds \tag{2.15}$$

(see [13] for examples). This higher order mode decomposition of a field is the computationally intensive step but it only has to be carried out once if there is no scattering of power between modes (if mirrors and lenses are treated as perfect phase transformers with no truncation). Optical elements can, however, introduce a significant amount of power scattering between modes as described in the next section.

The choice of the optimum beam mode set (in terms of the parameters W and R) is crucial to the efficiency of the Gaussian beam mode approach and several approaches can be taken. Very often a source field can be represented to a high accuracy by the sum of only a few modes and the mode set that maximises the power in the fundamental is chosen. In some cases, however, this can cause the power in the higher order modes, although small, to be spread essentially over a large number of modes with the result that they are all required to accurately model the field. The choice of W might more usefully take into account the ability of the highest order mode to model the edge of the field. If we consider Gaussian–Hermite modes, for example, the final zero crossing of the nth mode is approximately given by $\sqrt{0.75n}/W$. Matching this to the extent of the field to be decomposed gives a value for W [45, 46]. R can be chosen to match the phase curvature of the field. Once the mode coefficients are known, it is straightforward to model the propagation of a beam by simply keeping track of the evolution of the beam width, the phase radius of curvature and the phase slippage between modes (using, for example, *ABCD* matrices).

2.5.2 Aberrations, Truncation, Beam Distortion

If the beam guide or optical coupling system is not perfect then there may be truncation and aberration effects which distort the field [46–50]. It is also possible to have

a mismatched or defocussed beam as discussed above (Sect. 2.4.2). A propagating beam in an non-ideal quasi-optical system can be analysed in terms of what happens to its component modes and the non-ideal propagation can be viewed as resulting in the mode coefficients for the beam varying with propagation, a process we call scattering. There may also be some partial reflections present resulting in power travelling both in the forward and reverse directions through the optical system. For the case where we are concerned with the coupling of beams not well described by a Gaussian we can readily include higher order modes, which of course complicates the description but provides a higher level of accuracy in the analysis.

$$C_{ab} = \left| \int\int \sum_i A_i^* E_i^*(x, y; W_a, R_a) \sum_{i'} B_i E_{i'}(x, y; W_b, R_b) \mathrm{d}x\mathrm{d}y \right|^2$$
$$= \left| \sum_{ii'} A_i^* B_{i'} I_{ii'} \right|^2 \tag{2.16}$$

where $I_{ii'} = \int\int E_i^*(x, y; W_a, R_a) E_{i'}(x, y; W_b, R_b) \mathrm{d}x\mathrm{d}y$, [51, 52].

When designing a millimetre or THz quasi-optical system it is important, particularly in terms of truncation and vignetting, to know at what radius the propagating beam can be truncated without losing power (by a stop, edge of a mirror, lens, etc.). If the stop is in the far field of a source (such as a horn antenna feed) this can be straightforward as we can integrate the far-field beam pattern over the region defined by the stop. However, if the beam has been re-focussed and re-collimated a number of times, the beam pattern is no longer immediately obvious particularly in terms of its sidelobe structure at that plane. This can be very conveniently analysed using higher order Gaussian beam modes [53, 54]. The azimuthally symmetric Gaussian–Laguerre modes above (Sect. 2.5.1) are useful, for example, if the stop has circular symmetry and the propagating beam can be expressed efficiently in terms of the same modes.

Such effects can also be described by a scattering matrix **S** for the optical system which expresses how the component modes E_i are scattered by the optical system so that on a transverse output plane: $E_j^{\mathrm{sc}} = \sum_i S_{ij} E_i$. Any incident beam can be expressed as a coherent sum of such modes $E_{\mathrm{in}} = \sum_j A_j E_j$, so that the scattering matrix then acts on the mode coefficients, with the transmitted field mode coefficients given by: $B_i = S_{ij} A_j$. Thus, the transmitted field is expressed in terms of a different set of mode coefficients for non-ideal propagation $E_{\mathrm{out}} = E_{\mathrm{in}}^{\mathrm{sc}} = \sum_m B_i E_i$. We can express the evolution of the modes coefficients from A_i to B_i in matrix notation as $\mathbf{B} = \mathbf{S}.\mathbf{A}$. In certain cases a quasi-analytical approach can be taken. Thus, for example, if the beam is symmetrically truncated for a cylindrically symmetric system useful recursion relationships can be derived [54]. In the case of aberrating systems plotting mode amplitudes allows the Gaussicity (the pure simple Gaussian mode content in power) and higher order structure to be investigated.

A Gaussian beam mode analysis can be applied to any quasi-optical system in which there are partial reflections by also including the backward travelling modes (z and $R(z)$, change sign in Eq. (2.2)). Such reflections have the potential to set up standing waves in the system [55]. A full scattering matrix formulation can incorporate backward-going waves by considering a quasi-optical component as a two-port device with incident fields on port 1 and 2 described by sets of mode coefficients **A** and **C**, respectively, then the corresponding reflected fields are given by sets of coefficients **B** and **D**

$$\begin{bmatrix} \mathbf{B} \\ \mathbf{D} \end{bmatrix} = \begin{bmatrix} \mathbf{S}_{11} & \mathbf{S}_{12} \\ \mathbf{S}_{21} & \mathbf{S}_{22} \end{bmatrix} \begin{bmatrix} \mathbf{A} \\ \mathbf{C} \end{bmatrix}. \tag{2.17}$$

and the individual scattering matrices are calculated from the overlap integrals of the appropriate transmitted and reflected fields.

We calculate the scattering matrix for the overall system by cascading the scattering components appropriately. Thus, we get the total transmission to the output port and reflection back at the input port for the system as a whole. Furthermore, in horn antenna fed systems it is straightforward to combine a scattering matrix description of a horn antenna using waveguide modes with that for a quasi-optical system based on Gaussian beam modes, and we can model the standing waves between two horn antennas as discussed in [56].

Alternatively, the scattering matrix can be re-cast in terms of transmitted fields as

$$\begin{bmatrix} \mathbf{D} \\ \mathbf{C} \end{bmatrix} = \begin{bmatrix} \mathbf{T}_{11} & \mathbf{T}_{12} \\ \mathbf{T}_{21} & \mathbf{T}_{22} \end{bmatrix} \begin{bmatrix} \mathbf{A} \\ \mathbf{B} \end{bmatrix} = \begin{bmatrix} \mathbf{S}_{21} - \mathbf{S}_{22}\,[\mathbf{S}_{12}]^{-1}\,\mathbf{S}_{11} & \mathbf{S}_{22}\,[\mathbf{S}_{12}]^{-1} \\ -\,[\mathbf{S}_{12}]^{-1}\,\mathbf{S}_{11} & [\mathbf{S}_{12}]^{-1} \end{bmatrix} \begin{bmatrix} \mathbf{A} \\ \mathbf{B} \end{bmatrix}, \tag{2.18}$$

and sequential matrices can again be multiplied directly to model a system with multiple components. (Singular value decomposition can be used, if necessary, to invert the $\mathbf{S}_{12}$ scattering matrix, using the singular values to keep only the modes that are not truncated [45, 46]).

One of the limitations of Gaussian beam mode analysis is that polarisation effects in particular are not strictly speaking included in the theory which is a paraxial scalar theory. It is possible to include polarisation effects approximately, however, by defining two sets of orthogonally polarised modes (as discussed in [7, 12] for example and utilised in several papers on the Gaussian Beam Mode Analysis of horn antennas, e.g. [43]). It should be noted however that the scattering between co-polar and cross-polar fields cannot be rigorously included in the theory. In the case where more accurate polarisation behaviour is required therefore, other modelling techniques have to be applied as discussed in the next section.

2.5.3 Other Modelling Techniques

Optical modelling is concerned with the problem of calculating an electromagnetic field over a surface in an optical system when the field, or currents, over some other

surface is known. Techniques such as the Method of Moments [57] attempt to calculate the current distribution over a surface precisely but the full solution to Maxwell's equations is usually extremely difficult to find and in practice approximations have to be made. In the physical optics (PO) approximation made by the software package GRASP [58], for example, when a field is incident upon an aperture it is assumed that the field over the opaque region is zero and the field over the transparent region is the same as if no aperture were there. This is a reasonable approximation to make when the radius of curvature of the reflector is many wavelengths, but is not valid at an edge. The geometrical theory of diffraction (GTD), therefore, is often used in addition to geometrical optics (GO) to estimate the effect of aperture edges on the sidelobes. The PO technique is extremely powerful and is standard for analysing antennas and reflectors in radio and submillimetre systems.

The electromagnetic field over an input surface is a vector field but in some cases considering only one component of the field leads to relatively simple scalar solutions. For THz systems the question of whether a vector or a scalar solution is required is intrinsically related to whether the field is of a paraxial or wide-angle nature. In practice, when considering narrow-angle paraxial beams, it is sufficient to consider the components of the vector field separately. Propagation of the field onto the next optical component (solving the wave equation) requires diffraction integrals to be calculated for each field point. Kirchhoff's approximation is the arithmetic average of the rigorous solutions when there is ambiguity over which vector quantity (**E** or **H**) is being analysed. The averaging process appears in the form of the well-known $(1 + \cos\theta)/2$ obliquity term. Rather than evaluating diffraction integrals directly, it is possible to decompose an assumed source field into modes, each a solution of the wave equation. Propagation to the next optical surface is usually straightforward and simply involves recombining scaled modes with an appropriate mode-dependent phase slippage term included. Commonly used mode sets include Gaussian beam modes as discussed here, Gabor modes [59] (used by the commercial software package ASAP [60], for example) and plane waves (used by the software packages Zemax [61], GLAD [62]). A plane wave analysis has the significant advantage that it is does not have to be limited to paraxial fields.

At optical wavelengths, away from boundary shadows and abrupt changes in intensity distribution, energy can be considered to be transported along curves, or light rays, obeying certain geometrical laws. For system design at visible wavelengths this technique is widely used and ray-tracing packages, such as CODE V [63] and Zemax have proved to be very successful. Ray-tracing can also be accurate for systems that are highly over moded. In the submillimetre and THz regimes, however, the wavelength is typically an appreciable fraction of component sizes and so cannot be neglected. Systems tend to be at most few-moded and often have a compact optical layout. In this regime diffraction effects are important and the approach of geometrical optics is inadequate.

2.5.4 Partial Coherence and Multi-Moded Systems

In a multi-moded quasi-optical system the radiation field will be partially spatially coherent. Each true component mode of propagation, although having no fixed phase relationship with other modes, will of course propagate according to the laws of diffraction and the total field intensity at any point will be given by the sum of the intensities of these component modes (fields add in quadrature). Geometrical optics can be employed in highly over-moded systems as an efficient accurate approach. However, in the long-wavelength limit systems tend to be at most few moded and an approach incorporating diffraction techniques is necessary. When this is applied to a modal approach, for example, propagation can be very elegantly described in terms of coherence matrices. These track the evolution of the mutual coherence function [64, 65]. Over moded horn antennas can be used to couple to such beams [66–68].

2.6 Design of Optical Systems

2.6.1 Choice of Mirror/Lens Parameters

In many cases we wish to design a quasi-optical system that couples one beam (such as that produced by a feed horn antenna) to another (determined by a receiver system, for example). If the desired input and output beam waists are $W_{0,\text{out}}$ and $W_{0,\text{in}}$, respectively, then the magnification of the system is given by $\mathcal{M} = W_{0,\text{out}}/W_{0,\text{in}}$. If the separation of the beam waists is a free parameter then the distances d_{in} and d_{out} of the input and output waists, respectively, are given by

$$d_{\text{in}} = f \pm \mathcal{M}^{-1}\left[f^2 - f_0^2\right]^{0.5} \quad \text{and} \quad d_{\text{out}} = f \pm \mathcal{M}\left[f^2 - f_0^2\right]^{0.5}, \tag{2.19}$$

where

$$f_0 = \frac{\phi W_{0,\text{in}} W_{0,\text{out}}}{\lambda}. \tag{2.20}$$

We are free to choose the focal length of the system but it must have a minumum value of $f = f_0$. The choice of f determines the input and output distances and in the case where $f = f_0$, $d_{\text{in}} = d_{\text{out}} = f$ (independent of wavelength). Often, however, the distances between the beam waists, $d = d_{\text{in}} + d_{\text{out}}$, is fixed and therefore is the focal length. For $\mathcal{M} \neq 1$

$$f = \frac{\pm\left[(\mathcal{M} - \mathcal{M}^{-1})^2 f_0^2 + d^2\right]^{0.5}(\mathcal{M} + \mathcal{M}^{-1}) - 2d}{(\mathcal{M} - \mathcal{M}^{-1})^2}, \tag{2.21}$$

while for $\mathcal{M} = 1$

$$f = \frac{d}{4} + \frac{f_0^2}{d}. \tag{2.22}$$

These and other examples of Gaussian beam transformations are discussed in Goldsmith [3]. Once the component focal lengths and separations have been fixed a simple *ABCD* matrix analysis of an equivalent on-axis system (approximating the focussing elements by thin lenses of focal length f) can be performed in order to determine the beam waist, W, and radii of curvature, R_{in} and R_{out} at each optical component. The component sizes required depend on the level of beam truncation that can be tolerated but component diameters of $4W$ (giving -35 dB edge taper) are typical. If an off-axis geometry is required then the angle-of-throw needed at each component and the radii of curvature can be used together with the equations in Sect. 2.3.2 to define the reflecting surface. Although a geometrical optics design and analysis software packages can help with the initial layout of systems, a diffraction analysis (such as Gaussian beam modes) must be used to check minimum component sizes. If the optical system is to be used over a wide bandwidth then the beam-mode analysis should be carried out at a few wavelengths across the band as only in certain cases are beamwidths, etc., independent of wavelength.

Gaussian beam modes can be used to assess an optical design in terms of its beam Gaussicity (fractional power coupling to a given beam radius and phase curvature). Once designed, a more rigorous PO analysis should be used to verify the system performance in terms of other parameters such as loss and polarisation behaviour.

2.6.2 Layout of Systems

Once a Gaussian beam-mode analysis of an equivalent on-axis system has been used to determine component parameters and sizes, the layout of the system can be chosen depending on more specific performance requirements. For on-axis systems truncation (Sect. 2.5), standing waves and blockage may be issues while for off-axis systems stray light, beam distortion (Sect. 2.5), cross-polarisation and shadowing may be of more concern.

An important consideration is the introduction by optical components of polarisation effects (again, Gaussian beam modes are typically assumed to describe one linear polarisation). The cross-coupling of orthogonal polarisations is known as cross-polarisation and it can be introduced into a beam after reflection from a curved focussing element. In certain circumstances (an axially symmetric reflector viewed on-axis) the cross-polar component can cancel but this is generally not the case when using off-axis mirrors, for example. Such cross-polarisation has been investigated by Gans [69] and Murphy [15] and for quadratic reflector surfaces the fraction of the power in an incident beam that is reflected into the cross-polar component is

$$P_{xp} = \frac{W_m^2}{4f^2}\tan^2\theta_i, \tag{2.23}$$

where W_m is the incident beam radius at the mirror, θ_i is its angle of incidence and f is the focal length of the mirror (twice that lost due to beam distortion). Instrumental polarisation effects arise even in lens-based on-axis systems. At each vacuum/dielectric interface (or in fact any surface with finite conductivity) there is a difference in transmission for radiation polarised perpendicular or parallel to the plane of incidence (given by the Fresnel coefficients) and this difference increases with increasing angle of incidence. The result is that an unpolarised source may be detected as being polarised after transmission through the optical system. This may be true even for anti-reflection coated lenses if the optics are used at high angles of incidence or for signals of large bandwidth.

Partial reflections and standing waves are also issues for quasi-optical systems, in particular those with on-axis components (lenses, dielectric cryostat windows, central blockages, etc.). Partial reflections from interfaces can give rise to return loss and standing waves [55, 56]. These standing waves are particularly troublesome in spectrometers where they can appear as a baseline ripple in spectra. In addition, truncation and aberration effects in real optical components can be expected to scatter power between modes and modal resonances can occur when even a small amount of power is scattered into a higher order mode and that mode becomes trapped [70].

2.6.3 Issues for Imaging in THz Spectroscopy Systems

Most standard time-domain spectroscopy systems used in the laboratory operate in transmission and collimate or re-focus the THz beam using off-axis parabolic mirrors [71]. Reflection of the diverging beam from a source by a single parabolic mirror gives rise to distortion of the beam amplitude pattern, with beam squint because of projection effects [15]. For a pure Gaussian source the reduced Gaussicity of the distorted beam (fractional power coupling to a pure Gaussian) is given by

$$P_G = 1 - \frac{W_m^2}{8f^2}\tan^2\theta_i, \tag{2.24}$$

where W_m is again the beam width parameter at the mirror, f is the focal length of the mirror and θ_i is the angle of incidence.

However, if a focussed beam is required, then by an appropriate compensating Gaussian beam telescope arrangement of two identical parabolic mirrors it is possible to eliminate this distortion [48]. The focal length of the mirrors should be long enough that a collimated beam (with width parameter W_m) is formed between the parabolic mirrors (with $W_m \gg W_0$, the waist size at the source). At THz frequencies this is not difficult to achieve for typical source beams. The two parabolic surfaces provide the required phase transformations, while the correct relative orientations, as shown in Fig. 2.8, result in cancellation of the amplitude distortions. Then if the phase centre of the source antenna is located at the input focal plane of the first mirror, an essentially undistorted image of this field with a planar wave front (i.e. a waist) is produced at the

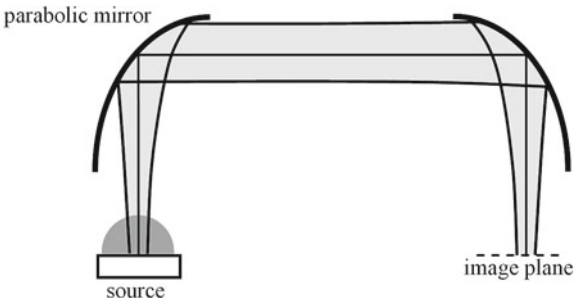

Fig. 2.8 Compensated arrangement of parabolic mirrors

output focal plane of the second mirror to illuminate the sample to be investigated, for example. A second similar compensated arrangement of a pair of parabolic mirrors can be used to produce an image of the sample at the detector plane by raster scanning (e.g. [71, 72]). However, the alignment of off-axis parabolic mirrors in these set ups is highly sensitive to the generation of unexpected aberrations. A similar set up can be arranged for reflection measurement systems [73].

For a broadband pulse the width of the illuminating spot (waist) at the sample will be frequency dependent, this clearly being determined by the frequency dependence of the source antenna scheme. Generally for the source and detector, photoconductive planar lens antennas are employed. The beams produced by these structures are not as well behaved nor indeed as well understood as the horn antenna feeds referred to above in Sect. 2.4.1. Useful discussions are given in Jepsen [74] and Rudd [75]. However, it is clear from these studies that there is a strong wavelength dependence of the beam source waist size [1, 74]. Thus, the illuminating beam at the sample in a Gaussian beam telescope arrangement will also be strongly frequency dependent.

If the sample is thick then diffraction in the sample may be significant and the optical path length through the sample needs to be taken into account in any optical design. The distance to the next focussing element can be adjusted accordingly to ensure that the phase centre of the beam scattered by the sample is positioned at the input focal plane of the second pair of parabolic mirrors so that an image of the sample is still formed at the detector plane. The *ABCD* matrix for propagation through the sample including the effects of refraction at the air-medium interfaces is given by $((1, t/n), (0, 1))$, where n is the refractive index and t is the thickness of the sample. Thus, the distance to the first parabolic mirror should be adjusted by $t(1 - 1/n)$.

2.7 Summary and Conclusions

The THz portion of the electromagnetic spectrum is a challenging one in which to work, as although radiation is typically propagated and analysed as free-space beams, unlike traditional optics, beams may be only a few wavelengths in diameter and diffraction effects are important. The Gaussian beam mode analysis described

here is a useful compromise between the vector physical optics analyses that are feasible at radio wavelengths and the ray-tracing techniques that have proven so successful at visible wavelengths.

Often a simple Gaussian amplitude distribution is a good approximation both to the radiated beam produced by a typical THz source and to the reception pattern of a typical detector feed. A Gaussian mode, since it is a solution to the paraxial wave equation, retains its amplitude distribution as it propagates and simply scales in beam width and phase-front radius of curvature. For multi-element optical systems we can use the convenient *ABCD* ray-transfer matrix formalism from geometrical optics to keep track of the beam parameters and to design compact and efficient optical systems. There are situations when we need to model more complex field distributions and in these cases we can use higher order beam-mode solutions, again for a paraxial regime. These higher order Gaussian modes are characterised by the same beam radius and phase radius of curvature as the fundamental mode, but slip in phase with respect to it as they propagate. This phase slippage can also be calculated from the *ABCD* matrix of an optical component. Indeed since Gaussian beam modes are the natural modes with which to describe propagation of quasi-collimated long-wavelength beams, only a small number of modes are required for many practical applications.

Gaussian beams can be re-collimated in a beam guide using re-focussing elements such as simple thin lenses or mirrors. Care must be taken, however, as the usual formulas for imaging in geometrical optics cannot be used in long-wavelength systems to predict the position of beam waists. Again *ABCD* matrices can be very useful in this regard. We have described focussing elements and some other optical components commonly used in long-wave optics such as polarising grids, roof mirrors and phase gratings. If a beam guide or optical coupling system is not perfect then there may be truncation and aberration effects which distort the field. Off-axis ellipsoidal and paraboloidal mirrors in particular are often used and these can introduce significant aberrations and extra diffraction effects across the beam; thus, very careful optical design is crucial for good performance.

A propagating beam in a non-ideal quasi-optical system can be analysed in terms of what happens to its constituent modes. Then non-ideal propagation can be viewed as resulting from power being scattered between these modes. There may also be some partial reflections present in a system resulting in power travelling both in the forward and reverse directions. We have discussed how both partial reflections and the scattering of power between modes can be described using Gaussian mode scattering matrices. Furthermore, Gaussian beam mode techniques can also be extended to model incoherent and partially coherent fields.

One of the limitations of Gaussian beam mode analysis is that polarisation effects such as the scattering between co-polar and cross-polar fields cannot be rigorously included in what is a paraxial scalar theory. In the case where the accurate polarisation behaviour is required other modelling techniques, such as physical optics, should be used.

In conclusion, in this chapter we have discussed the design and analysis of THz beam guides and optical coupling systems, including an overview of the large range

of typical quasi-optical components. A powerful and efficient approach to modelling propagation based on Gaussian beam mode analysis has been developed which has proved invaluable for the reliable design and optimisation of the performance of the unique optical systems encountered in the THz band.

References

1. Y-S. Lee, *Principles of Terahertz Science and Technology* (Springer, New York, 2009)
2. P.F. Goldsmith, Proc. IEEE **80**, 1729 (1992)
3. P.F. Goldsmith, *Quasioptical Systems* (IEEE Press, New York, 1998)
4. L. Diaz, T. Milligan, *Antenna Engineering Using Physical Optics: Practical CAD Techniques and Software* (Artech House, Boston, 1996)
5. A.E. Siegman, in *Lasers* (University Science Books, Mill Valley, 1986)
6. P.F. Goldsmith, in *Infrared and Millimeter Waves*, vol. 6, ed. by K.J. Button (Academic Press, NewYork, 1982)
7. D.H. Martin, J.W. Bowen, IEEE Trans. Microw. Theory Tech. **41**, 1676 (1993)
8. J.C.G. Lesurf, *Millimetre-Wave Optics, Devices and Systems* (Adam Holger, Bristol, 1990)
9. G. Goubau, in *Millimetre and Submillimetre Waves*, ed. by F.A. Benson (Illfe Press, London, 1969)
10. H. Kogelnik, T. Li, Proc. IEEE **54**, 1312 (1966)
11. S. Ramo, J.R. Whinnery, T. Van Duzer, *Fields and Waves in Communication Electronics*, 3rd edn. (Wiley, New York, 1994)
12. J.A. Murphy, IEEE Trans. Antennas Propag. **36**, 570–574 (1988)
13. J.A. Murphy, A. Egan, Eur. J. Phys. **14**, 121–127 (1993)
14. S. Withington, J.A. Murphy, K.G. Isaak, Infrared Phys. Technol. **36**, 723 (1995)
15. J.A. Murphy, Int. J. IR Millim. Waves **8**, 1165 (1987)
16. K. Wang, D.M. Mittelman, Nature **432**, 376 (2004)
17. R.J. Mahon, J.A. Murphy, W. Lanigan, Opt. Commun. **260**, 469 (2006)
18. A. Tamminen, J. Ala-Laurinaho, A.V. Räisänen, Indirect holographic imaging at 310 GHz, Proceeding of the 5th European Radar Conference, 2008, pp. 168–171
19. B. Maffei, F. Noviello, J.A. Murphy et al., Astron. Astrophys. (Pre-launch status of the Planck mission: Special feature), **520**, A11 (2010)
20. C. Dragone, Bell Syst. Tech. J. **57**, 2663 (1978)
21. J. Lau et al., Appl. Opt. **45**, 3746–3751 (2006)
22. J.W. Fowler, Appl. Opt. **46**, 3444 (2007)
23. D.H. Martin, E. Puplett, Infrared Phys. **10**, 105 (1969)
24. R. Padman, Int. J. Infrared Millim. Waves **13**, 1487 (1992)
25. P.F. Goldsmith, IEEE Trans. Antennas Propag. **39**, 834 (1991)
26. M. Beruete et al., IEEE Microw. Wirel. Compon. Lett. **17**, 834 (2007)
27. B. Rulf, Am. J. Phys. **56**, 76 (1988)
28. T. Finn, N. Trappe, J.A. Murphy, J. Opt. Soc. Am. A **25**, 80 (2008)
29. P.A.R. Ade, G. Pisano, C. Tucker, Proc. SPIE **6275**, 62750U (2006)
30. D.C. O'Shea, Th.J Suleski, A.D. Kathman, D.W. Prather, *Diffractive Optics Design, Fabrication, and Test*, (Tutorial Texts in Optical Engineering), vol. TT62 (SPIE Press, Washington, 2004)
31. H. Dammann, E. Klotz, Opt. Acta **24**, 505 (1977)
32. J.A. Murphy, C. O'Sullivan, N. Trappe, W. Lanigan, R. Colgan, S. Withington, Int. J. IR Millim. Waves **20**, 1469 (1999)
33. R. May, Proc. SPIE **6893**, G8930 (2008)
34. H. Kim, B. Yang, B. Lee, J. Opt. Soc. Am. A **21**, 2353 (2004)

35. E. Johnson, M. Abushagur, J. Opt. Soc. Am. A **12**, 1152 (1995)
36. J. Lavelle, C. O'Sullivan, J. Opt. Soc. Am. A **27**, 350 (2010)
37. J. Durnin, J. Opt. Soc. Am. A **4**, 651 (1987)
38. S. Monk, J. Arlt, D. Robertson, J. Courtial, M. Padgett, Opt. Commun. **170**, 213 (1999)
39. N. Trappe, R. Mahon, W. Lanigan, J.A. Murphy, S. Withington, Infrared Phys. Technol. **46**, 233 (2005)
40. R.J. Wylde, Proc. IEE Part H **131**, 258 (1984)
41. R.J. Wylde, D.H. Martin, IEEE Trans. Microw. Theory Tech. **41**, 1691 (1993)
42. J.A. Murphy, R. Padman, R.E. Hills, Int. J. IR Millim. Waves **9**, 325 (1988)
43. S. Withington, J.A. Murphy, IEEE Trans. Antennas Propag. **40**, 198 (1992)
44. W.B. Joyce, B.C. DeLoach, Appl. Opt. **23**, 4187 (1984)
45. D. White, Dissertation, National University of Ireland Maynooth, 2006
46. M.L. Gradziel, C. O'Sullivan, J.A. Murphy et al., Proc. SPIE **6472**, D4720 (2007)
47. A. Yoshida, T. Asakura, Opt. Commun. **25**, 133 (1978)
48. J.A. Murphy, S. Withington, Infrared Phys. Technol. **37**, 205 (1996)
49. N. Trappe, J.A. Murphy, S. Withington, Eur. J. Phys. **24**, 403 (2003)
50. T. Finn, N. Trappe, J.A. Murphy, S. Withington, Infrared Phys. Technol. **51**, 351 (2008)
51. J.A. Murphy, M. McCabe, S. Withington, Int. J. IR Millim. Waves **18**, 501 (1997)
52. H. Jiang, D. Zhao, Optik **117**, 215 (2006)
53. J.A. Murphy, A. Egan, S. Withington, IEEE Trans. Antennas Propag. **41**, 1408 (1993)
54. J.A. Murphy, S. Withington, A. Egan, IEEE Trans. Microw. Theory Tech. **41**, 1700 (1993)
55. J.A. Murphy, N. Trappe, S. Withington, Infrared Phys. Technol. **44**, 289 (2003)
56. N. Trappe, J.A. Murphy, S. Withington et al., IEEE Trans. Antennas Propag. **53**, 1755 (2005)
57. R.F. Harrington, *Field Computation by Moments Methods* (Mac Millan, New York, 1968)
58. TICRA Engineering Consultants, GRASP9, http://www.ticra.dk/
59. P.D. Einziger, S. Raz, M. Shapira, J. Opt. Soc. Am. A **3**, 508 (1986)
60. Breault Research Organization (BRO), http://www.breault.com/software/asap.php
61. ZEMAX Development Corporation, Zemax-EE, http://www.zemax.com/
62. G. Lawrence, SPIE no. 766–18, O-E/Lase, 1987
63. Code, V, Optical Research Associates, http://www.opticalres.com/cv/cvprodds_f.html
64. S. Withington, J.A. Murphy, IEEE Trans. Antennas Propag. **46**, 1650 (1998)
65. S. Withington, G. Yassin, J.A. Murphy, IEEE Trans. Antennas Propag. **49**, 1226 (2001)
66. R. Padman, J.A. Murphy, Infrared Phys. **31**, 441 (1991)
67. E. Gleeson, J.A. Murphy, B. Maffei et al., Infrared Phys. Technol. **46**, 493 (2005)
68. J.A. Murphy, T. Peacocke, B. Maffei et al., JINST **5**(Art. No. T04001), (2010)
69. M.J. Gans, Bell Syst. Tech. J. **55**, 289 (1976)
70. P.A.S. Cruickshank, D.R. Bolton, D.A. Robertson, R.J. Wylde, G.N. Smith, in *Proceeding of The Joint 32nd International Conference on Infrared and Millimeter Waves and 15th International Conference on Terahertz Electronics*, Cardiff, 3–7 September, 2007, vol. 2, pp. 941–942
71. W.L. Chan, J.A. Deibel, D.M. Mittleman, Rep. Prog. Phys. **70**, 1325 (2007)
72. P.C.M. Planken, H.J. Bakker, Appl. Phys. A Mater. Process. **78**, 465 (2004)
73. S. Huang, P.C. Ashworth, K.W. Kan, Y. Chen, V.P. Wallace, Y-t Zhang, E. Pickwell-MacPherson, Opt. Express **17**, 3848 (2009)
74. P. Uhd Jepsen, R.H. Jacobsen, S.R. Keiding, JOSA B **13**, 2424 (1996)
75. J. Van Rudd, D.M. Mittleman, JOSA B **19**, 319 (2002)

http://www.springer.com/978-3-642-29563-8

Terahertz Spectroscopy and Imaging
Peiponen, K.-E.; Zeitler, A.; Kuwata-Gonokami, M. (Eds.)
2013, XXXII, 644 p., Hardcover
ISBN: 978-3-642-29563-8